Symmetry breaking in a 3D bluff-body wake

By G. Rigas†, L. Esclapez AND L. Magri

The dynamics of a three-dimensional axisymmetric bluff-body wake are examined at low Reynolds regimes where transitions take place through spatio-temporal symmetry breaking. A linear stability analysis is employed to identify the critical Reynolds number associated with symmetry breaking, and the associated eigenmodes, known as global modes. The analysis shows that the axisymmetric stable base flow breaks the rotational symmetry through a pitchfork $m = 1$ bifurcation, in agreement with previously reported results for axisymmetric wakes. Above this threshold, the stable base flow is steady and three-dimensional with planar symmetry. A three-dimensional global stability analysis around the steady reflectionally symmetric base flow, assuming no homogeneous directions, predicts accurately the Hopf bifurcation threshold, which leads to asymmetric vortex shedding. DNS simulations validate the stability results and characterize the flow topology during the early chaotic regime.

1. Introduction

Bluff-body flows are of fundamental importance to many industries, in particular the transport industry, where the aerodynamic drag arising from such flows can be the dominant source of vehicle fuel-burn and CO_2 emissions. Recent advances in hydrodynamic stability have further aided understanding and controling laminar and transitional regimes (Sipp *et al.* 2010; Luchini & Bottaro 2014; Sipp & Schmid 2016), particularly for two-dimensional (2D) flows. However, flows of practical and industrial interest involve three-dimensional (3D) wakes and high Reynolds numbers. Despite their turbulence and complexity, such flows exhibit organization, which manifests as coherent flow structures. These structures are usually associated with increased noise, structural fatigue and drag.

During the transitional regime of laminar wakes, continuous spatial and temporal symmetries are spontaneously broken through a sequence of bifurcations. Specifically, the axisymmetric 3D wake undergoes a steady bifurcation followed by an unsteady one with azimuthal wavenumbers $|m| = 1$ at low Reynolds numbers prior to the emergence of chaos (Fabre *et al.* 2008; Meliga *et al.* 2009; Bohorquez *et al.* 2011; Bury & Jardin 2012). These bifurcations break spatial-rotational and time-translation symmetries, giving rise to a reflectionally symmetric steady flow and unsteady vortex shedding. Similar transitional behavior has also been observed in 3D bluff bodies with reflectional symmetries, such as square plates (Marquet & Larsson 2015).

Perhaps surprisingly, it was shown recently that the turbulent dominant dynamics of 3D wakes can be linked to the hydrodynamic instabilities observed during the transitional regimes at low Reynolds numbers, including axisymmetric geometries (Rigas *et al.* 2014, 2015) and square ones, such as the Ahmed body (Grandemange *et al.* 2013). Understanding the wake dynamics in the laminar and transitional regimes is paramount for the development of control strategies, which can be appropriately extended to turbulent cases (Brackston *et al.* 2016).

† Mechanical and Civil Engineering Department, California Institute of Technology

In this study, global linear stability analysis (LSA) and direct numerical simulation (DNS) are employed to study the intrinsic dynamics leading to chaotic/turbulent behavior in a 3D axisymmetric bluff-body wake. The remainder of this paper is structured as follows. Section 2 briefly outlines the computational set-up. Section 3 presents the predictions of the LSA. Section 4 describes the transitional regimes obtained from DNS. Finally, conclusions are drawn in Section 5.

2. Computational setup

The geometry employed in this study is a 3D axisymmetric bluff body (Figure 1) with a blunt trailing edge, which has been studied experimentally in Rigas *et al.* (2014, 2015) and Oxlade *et al.* (2015). The length-to-diameter ratio, L/D, is 6.48. The bluff-body nose employs a modified super-ellipsoid with an aspect ratio $AR = 2.5$, given by the revolution of $y = (1 - z/AR)^m + y^2 = 1$, $0 < z < AR$, $m = 2 + (z/AR)^2$ around the centerline (Lin *et al.* 1992). Cylindrical (r, θ, z) and Cartesian (x, y, z) coordinates with the origin taken at the center of the base of the body are used in the subsequent analysis.

2.1. *Stability calculations*

The fluid motion is governed by the incompressible Navier-Stokes (NS) equations

$$\partial_t \mathbf{u} + \mathbf{u} \cdot \nabla \mathbf{u} + \nabla p - \mathrm{Re}^{-1} \nabla^2 \mathbf{u} = 0, \qquad \nabla \cdot \mathbf{u} = 0. \tag{2.1}$$

In the stability analysis, $\mathbf{u} = (u_r, u_\theta, u_z)^T$ where u_r, u_θ, u_z are the radial, azimuthal and axial components of the velocity. The stability analysis examines the evolution of infinitesimal perturbations around fixed-point solutions of (2.1), known as base flows.

The base flow $\mathbf{q}_0 = (\mathbf{u}_0, p_0)^T$ is a steady solution of the NS equations

$$\mathbf{u_0} \cdot \nabla \mathbf{u_0} + \nabla p_0 - \mathrm{Re}^{-1} \nabla^2 \mathbf{u_0} = 0 \ \text{ and } \ \nabla \cdot \mathbf{u_0} = 0. \tag{2.2}$$

The linear perturbation equations read

$$\partial_t \mathbf{u}' + \mathbf{u_0} \cdot \nabla \mathbf{u}' + \mathbf{u}' \cdot \nabla \mathbf{u_0} + \nabla p' - \mathrm{Re}^{-1} \nabla^2 \mathbf{u}' = 0 \ \text{ and } \ \nabla \cdot \mathbf{u}' = 0, \tag{2.3}$$

which, in compact form, read

$$\mathcal{B} \partial_t \mathbf{q}' + \mathcal{A} \mathbf{q}' = 0. \tag{2.4}$$

Assuming no homogeneous directions, the solutions are sought as normal modes with linear growth rate σ and frequency ω

$$\mathbf{q}' = \hat{\mathbf{q}}_{3D}(r, \theta, z) e^{(\sigma + i\omega)t} + c.c. \tag{2.5}$$

For an axisymmetric base flow, the azimuthal coordinate can be further Fourier-transformed in terms of the azimuthal wavenumber m, where m is an integer parameter, as

$$\mathbf{q}' = \hat{\mathbf{q}}_{2D}(r, z) e^{(\sigma + i\omega)t + im\theta} + c.c. \tag{2.6}$$

Substituting the normal-mode decompositions into Eq. (2.3) leads to 3D and 2D generalized eigenvalue problems with appropriate boundary conditions. These read

$$(\sigma + i\omega) \mathcal{B} \hat{\mathbf{q}} + \mathcal{A}_{(m)} \hat{\mathbf{q}} = 0. \tag{2.7}$$

For each global mode $\hat{\mathbf{q}}$ the correspondent adjoint mode $\hat{\mathbf{q}}^\dagger$ is computed from

$$(\sigma - i\omega) \mathcal{B}^\dagger \hat{\mathbf{q}}^\dagger + \mathcal{A}^\dagger_{(m)} \hat{\mathbf{q}}^\dagger = 0. \tag{2.8}$$

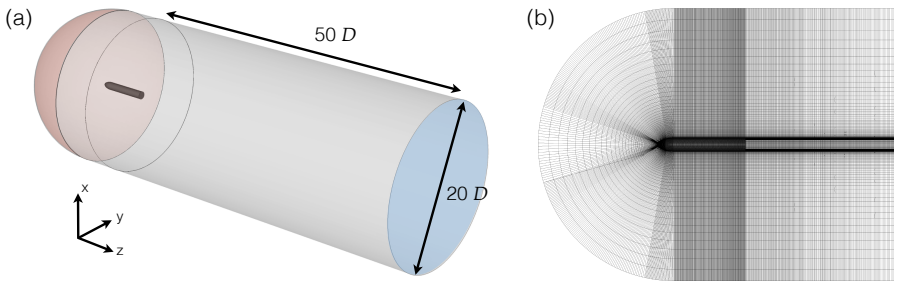

FIGURE 1. (a) DNS computational domain. (b) Mesh in a y-normal plane.

The adjoint operators can be either derived analytically from the direct equations (Eq. (2.3)), which is known as the continuous adjoint, or formed from the numerically discretized operator, which is known as the discrete adjoint (Luchini & Bottaro 2014). For this flow configuration and the numerical schemes adopted, the discrete-adjoint formulation is adopted. Hence, the adjoint operators are given by the complex conjugate of the discretized direct operators. The adjoint equations can be used to evaluate the effects of generic initial conditions and forcing terms on the time-asymptotic behavior of the system. Moreover, once the direct and adjoint modes are computed, the sensitivity of the global modes to local feedback (structural sensitivity, Giannetti & Luchini (2007)) and base-flow modifications (Bottaro *et al.* 2003; Marquet *et al.* 2008) can be examined.

The spatial discretization of the base flow and the linear equations is performed in the finite-element software FreeFem++ (Hecht 2012), interfaced with PETSc for parallel calculations, using a continuous Galerkin scheme with $P2-P1$ Taylor-Hood elements. Results presented here were obtained using an unstructured mesh with approximately 500,000 tetrahedra elements. The base-flow solution of the steady nonlinear equations (2.2) is obtained using an iterative Newton method and the direct linear solver MUMPS (Amestoy *et al.* 2001). Convergence is reached when the $\mathcal{L}_2$-norm of the residual of the governing equations becomes smaller than 10^{-12}. Eigenvalue problems (2D and 3D) are solved with SLEPc (Hernandez *et al.* 2005) using a shift-and-invert method.

2.2. *Direct numerical simulations*

The low-Mach-number solver VIDA (Cascade Technologies, Inc.) is used to solve the incompressible NS equations by setting constant density. It is a finite-volume, unstructured, massively parallel LES/DNS solver for reacting and non-reacting flows, fourth-order accurate in space and second-order accurate in time (Ham *et al.* 2007). The equations are solved in Cartesian coordinates, with z being the streamwise direction. Standard air properties at $T = 20^\circ$ C; $\nu = 15.11 \times 10^{-6}$ m^2/s; $\rho = 1.205$ kg/m^3 are utilized. The computational domain is shown in Figure 1(a): it consists of a 50-diameter $\times$ 20-diameter cylinder with a half-sphere inlet. A uniform velocity profile boundary condition is imposed at the inlet, no-slip at the bluff-body walls, convective at the outlet and slip conditions at the outer radial boundary. Several meshes of increasing spatial resolution were used and velocity statistics were found to converge with a mesh of about 5 million cells for Re up to 1000 and of about 10 million cells for higher Re. The former mesh has a grid point distribution in axial, radial and azimuthal directions of $300 \times 50 \times 60$ (Figure 1(b)), the latter has a grid point distribution of $600 \times 70 \times 120$.

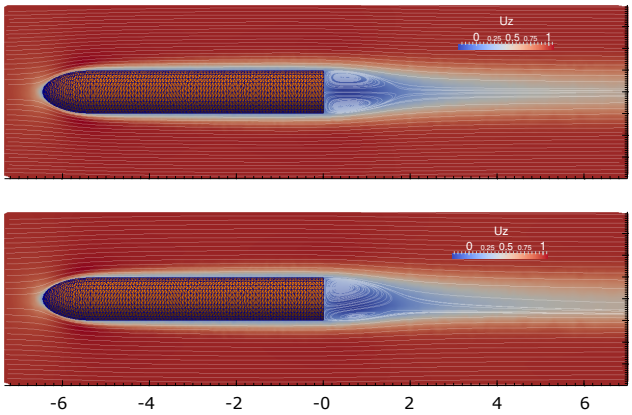

FIGURE 2. Base flows (fixed point solutions of the Navier-Stokes equations) at Re = 500. Streamwise velocity component U_z and streamlines in the xz plane. Top: rotationally symmetric (axisymmetric) base flow. Bottom: reflectionally symmetric base flow with respect to the xz plane.

3. Linear stability analysis

In the limit of vanishingly small Reynolds numbers, $\mathrm{Re} \ll 1$, the base flow is steady (time invariant) and axisymmetric (azimuthally invariant), respecting the axisymmetry of the bluff-body configuration. The flow is stable, which means that perturbations decay asymptotically in time i.e., all the eigenvalues of the linearized NS operator have strictly negative real part, $\sigma < 0$. En route to chaos, these symmetries break through a series of bifurcations that bring about reduced symmetry in space or time. The transition between the various symmetry groups is characterized here through LSA. For the flow studied in this paper, when a bifurcation occurs, the base flow (equilibrium) becomes unstable and a real eigenvalue (steady pitchfork bifurcation) or a complex conjugate pair (unsteady Hopf bifurcation) attains positive growth rates ($\sigma > 0$).

The first symmetry-breaking bifurcation is a steady bifurcation at $\mathrm{Re}_c = 424$, which breaks the rotational symmetry of the axisymmetric 2D base flow and leads to a 3D topology. Above this critical Reynolds number the axisymmetric base flow becomes unstable and a new stable base flow emerges. The stable base flow is characterized by reflectional symmetry in the azimuthal direction. These two equilibria for Re = 500 are shown in Figure 2. The growth rate and frequency obtained by examining the stability of these base flows are shown in Figure 3.

3.1. *Global modes of axisymmetric (2D) base flow*

Two bifurcations are identified by examining the stability of the axisymmetric flow and relevant global modes. At $\mathrm{Re}_c = 424$ the axisymmetric base flow undergoes a steady pitchfork bifurcation, with azimuthal wavenumber $m = 1$ and zero frequency ($\omega_c = 0$). At $\mathrm{Re}_c = 802$ the axisymmetric base flow undergoes an unsteady Hopf bifurcation, with azimuthal wavenumbers $m = \pm 1$. A complex conjugate pair of eigenvalues crosses the imaginary axis of the spectrum, with a critical Strouhal frequency of 0.075. The direct and adjoint eigenmodes for Re = 600 are shown in Figure 4(a,b).

The two symmetry-breaking bifurcations obtained from the stability of the axisymmetric base flow are in agreement with the findings of Sanmiguel-Rojas *et al.* (2011); Bohorquez *et al.* (2011) for an axisymmetric body of similar geometry. The threshold for the steady bifurcation is in agreement with the critical value 420, obtained from the

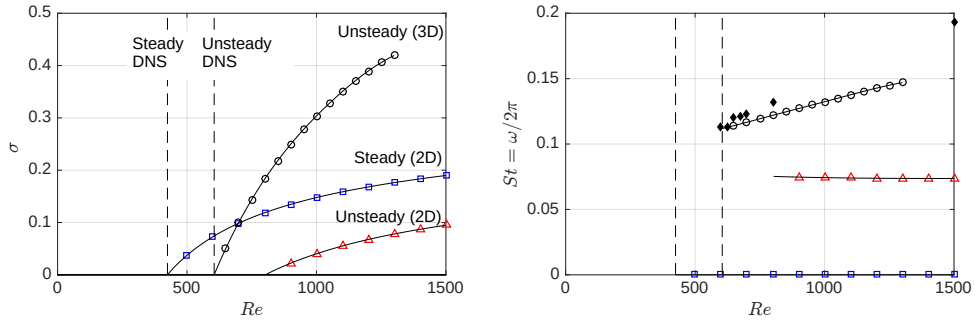

FIGURE 3. Growth rate (left) and frequency (right) of the most unstable global modes against Reynolds numbers. Steady mode (blue squares) and unsteady vortex shedding mode (red triangles) predictions using the axisymmetric 2D base flow. Unsteady vortex shedding mode using the reflectionally symmetric 3D base flow (black circles). Critical Re (dashed lines) and frequencies (filled symbols) from DNS.

DNS. However, the frequency and the critical Reynolds number for the unsteady vortex shedding do not match the DNS values. This is because the axisymmetric base flow has become unstable at a lower Re due to the steady bifurcation, thereby not serving as the correct base solution for predicting the Hopf bifurcation. For the same reason, this unsteady flow regime cannot be observed as a solution in the asymptotic time regime. An accurate prediction of the threshold and mode shape of the unsteady bifurcation requires the solution of the eigenvalue problem around the stable equilibrium, which is 3D, as explained in the next section.

3.2. *Global modes of reflectionally symmetric (3D) base flow*

The new emerging stable base flow for $\mathrm{Re}_c > 424$ is characterized by reflectional symmetry and is fully 3D. We find that at $\mathrm{Re}_c = 605$ the reflectionally symmetric base flow undergoes an unsteady bifurcation. A complex conjugate pair of eigenvalues crosses the imaginary axis, with a critical Strouhal frequency of 0.113. This is in agreement with the DNS values for the threshold (600) and frequency (0.113). The associated unstable unsteady global mode inherits the symmetry properties of the base flow, as shown in Figure 4(c), and becomes reflectionally symmetric, biased toward the same direction as the base flow.

The LSA is valid close to the threshold of the bifurcation (right panel of Figure 3). The frequency deviation between the DNS results and the linear stability for higher Re is due to the nonlinear base-flow modification caused by the Reynolds stresses associated with the global shedding mode. For an accurate prediction of the saturated frequency and amplitude of the global mode, a weakly nonlinear analysis (Sipp & Lebedev 2007; Meliga *et al.* 2009) or a self-consistent model (Mantič-Lugo *et al.* 2014) would be necessary. Note that the nonlinear base-flow modifications associated with the first steady mode above the threshold of the first bifurcation are fully accounted for here because of the appropriate choice of the stable reflectionally symmetric flow. For the stable and steady regimes, the axisymmetric base flow, $\mathrm{Re} < 424$, and the reflectionally symmetric base flow, $424 < \mathrm{Re} < 605$, obtained by the Newton-Raphson solver, are exact solutions of the NS equations and correspond to the mean flow, as found also with DNS. The advantages of using the Newton-Raphson solver over DNS are (i) the low computational cost because

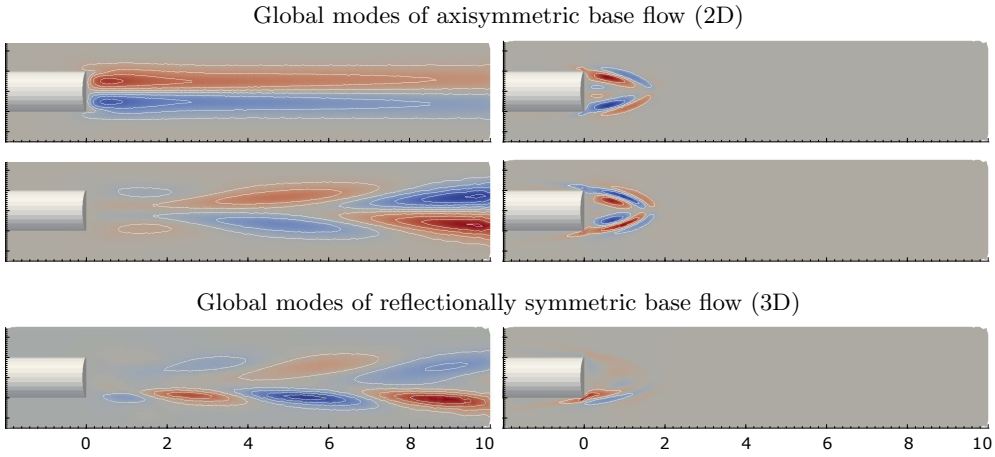

FIGURE 4. Global modes at Re = 600: direct (left) and adjoint (right). Steady symmetry breaking of the axisymmetric base flow (top); unsteady vortex shedding around the axisymmetric base flow (middle); (c) unsteady vortex shedding around the reflectionally symmetric base flow (bottom). The real part of streamwise velocity component is shown in the xz plane.

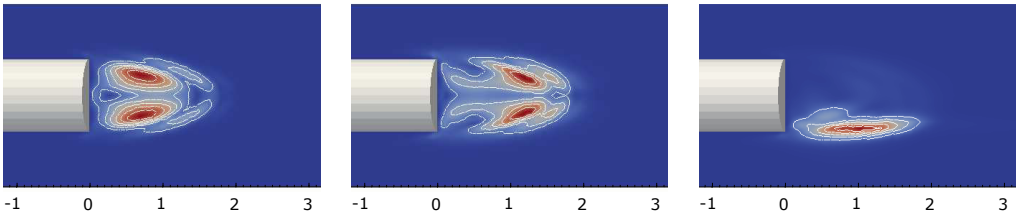

FIGURE 5. Structural sensitivity of the global modes shown in Figure 4.

the method converges after a few iterations, and (ii) the ability of obtaining unstable base flows with no further implementation.

3.3. *Structural sensitivity*

Mathematically, the structural sensitivity is related to the first-order sensitivity of an eigenvalue to small perturbations of the direct linear operator. When the direct operator, $\mathcal{A}$, is structurally perturbed by $\delta\mathcal{A}$, such that $\mathcal{A} \to \mathcal{A} + \varepsilon\delta\mathcal{A}$ and $\sigma \to \sigma + \varepsilon\delta\sigma$, the first-order drift of the eigenvalue is given by the Gâteaux derivative (Magri 2015)

$$\delta\sigma \equiv \lim_{\varepsilon \to 0} \left[\frac{\sigma\left(\mathcal{A} + \varepsilon\delta\mathcal{A}\right) - \sigma\left(\mathcal{A}\right)}{\varepsilon} \right]. \tag{3.1}$$

The resulting drifts in the eigenfunctions are assumed to be perturbed as $\hat{\mathbf{q}} \to \hat{\mathbf{q}} + \varepsilon\delta\hat{\mathbf{q}}$ and $\hat{\mathbf{q}}^\dagger \to \hat{\mathbf{q}}^\dagger + \varepsilon\delta\hat{\mathbf{q}}^\dagger$. By taking the limit $\varepsilon \to 0$ and using the bi-orthogonality condition, it can be shown that for linear eigenvalue problems (see, e.g., Giannetti & Luchini 2007)

$$\delta\sigma = \frac{\left\langle \hat{\mathbf{q}}^\dagger, \delta\mathcal{A}\hat{\mathbf{q}} \right\rangle}{\left\langle \hat{\mathbf{q}}^\dagger, \mathcal{B}\hat{\mathbf{q}} \right\rangle}, \tag{3.2}$$

where $\langle \cdot, \cdot \rangle$ is an inner product. (The extension of this formula for nonlinear eigenvalue problems can be found in Magri *et al.* (2016)). By considering a structural perturbation

that is localized in space by the identity tensor, we define the structural sensitivity of the direct operator, $\mathcal{A}$, as (Giannetti & Luchini 2007)

$$S(x,y,z) = \frac{\|\hat{\mathbf{u}}(x,y,z)\| \cdot \|\hat{\mathbf{u}}^\dagger(x,y,z)\|}{\langle \hat{\mathbf{q}}^\dagger, \mathcal{B}\hat{\mathbf{q}} \rangle}.$$

Physically, the region in the flow acting as a wavemaker in the excitation of the global instability can be identified by considering the structural sensitivity of the unstable mode. This concept, although typically used for oscillatory bifurcations, can be also used for examining the core region of instability due to a steady bifurcation. At the same time, it can provide directions for the implementation of passive and localized control strategies.

The structural sensitivities of the global modes identified from global LSA are shown in Figure 5. The maximum magnitude for the steady bifurcation lies inside the recirculation bubble. For the unsteady bifurcation computed around the axisymmetric base flow, the wavemaker region is located closer to the end of the recirculation bubble. Interestingly, for the reflectionally symmetric base flow, the sensitivity appears to move closer to the body and becomes asymmetric in accordance with the symmetry of the base flow.

4. Direct numerical simulations

DNS simulations are performed to investigate the transition stages to chaos and validate the LSA predictions. An overview of the simulations performed in terms of Reynolds number and spatio-temporal behavior is given in Table 1. The simulations span over the range between $\mathrm{Re} = 300$ and $\mathrm{Re} = 1500$. In Figure 6, instantaneous snapshots of the normalized streamwise vorticity $\omega_z^* = \omega_z D/w_\infty$ iso-contours for the various regimes are shown, in addition to the power spectral density (PSD) of the center of pressure at the base and half-diameter downstream.

For $\mathrm{Re} < 400$, the base flow is axisymmetric and steady (not shown here). At $\mathrm{Re} = 420$, the steady flow is asymmetric and the rotational symmetry is broken. The new flow topology is characterized by reflectional symmetry around a plane passing through the axis of the body. The angle of the symmetry plane is determined by the initial conditions. At $\mathrm{Re} = 550$, the side view in Figure 6 shows that the streamwise vortices are not aligned in the streamwise direction but exhibit an increasing eccentricity as the downstream distance from the base increases. The eccentricity increases with the Reynolds number and can be used to evaluate the Re_c of the steady bifurcation (Bohorquez *et al.* 2011).

For $\mathrm{Re} \geq 600$, the flow is unsteady and anti-symmetric vortices are shed periodically. A dominant single frequency appears in the PSD of the center of pressure. The LSA predictions are in agreement with the DNS.

For $\mathrm{Re} > 675$ the flow is aperiodic, presumably quasi-periodic, i.e., having two incommensurate frequencies, and multiple frequencies appear in the PSD. First, the higher harmonics of the vortex shedding become stronger. Second, a low-frequency peak at $St = 0.027$ is observed. The vortex shedding becomes irregular and bursts of vorticity occur approximately every 5 vortex shedding cycles, as shown in Figure 6. Interestingly, the wake preserves the reflectional symmetry. A fully nonlinear characterization of these solutions can be obtained by advanced techniques from time-series analysis (Hegger *et al.* 1999), such as phase-space reconstruction, recurrence analysis, Lyapunov analysis and entropy calculations. This is under way and will be reported in a separate paper.

For $\mathrm{Re} > 900$, high irregularity is observed in space and time. All the spatial and temporal symmetries of the flow are broken. The PSD of the fluctuations in the near

Temporal	Spatial	Re
Steady	Axisymmetric	300, 400
Steady	Reflectional symmetry	420, 430, 500, 550
Periodic	Reflectional symmetry	600, 625, 650
Aperiodic	Reflectional symmetry	675, 700, 750, 800
Chaotic	No symmetry	900, 1000, 1500

TABLE 1. Characterization of the DNS solutions for the Reynolds numbers investigated.

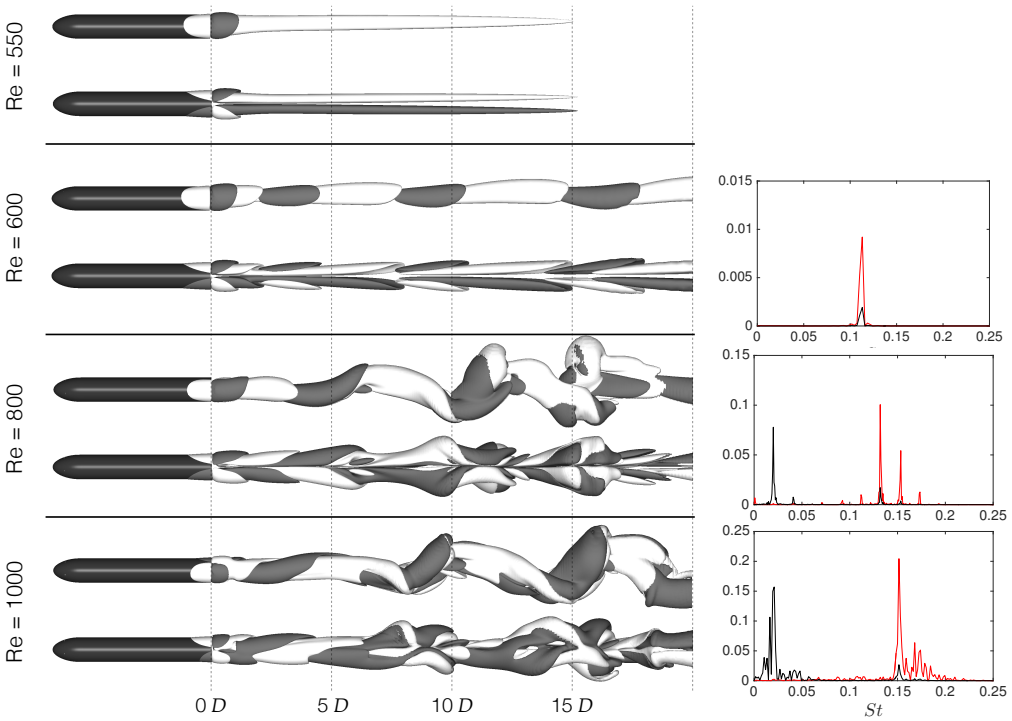

FIGURE 6. DNS simulations at Re: 550, 600, 800, 1000. Left: Streamwise vorticity contours, $\omega_z^* = \pm 0.05$, in the wake of the bluff-body; side (top) and plane (bottom) views. Right: Power spectral desnity (PSD) versus Strouhal number of the pressure barycenter on the base (black) and $0.5D$ downstream of the base (red) for the unsteady cases.

wake show rich energy content around the two main frequencies of the previous regime, and the energy of the higher vortex shedding harmonics has spread over a wide frequency range. For Re = 900, the Lyapunov exponents for this flow are calculated in Blonigan *et al.* (2016). One Lyapunov exponent is found positive, which indicates that the solution is low-dimensional chaotic. Furthermore, it is found that the irregular bursts observed above are associated with discrete peaks with positive finite-time Lyapunov exponent values, indicating the chaotic transition of the wake.

5. Conclusions

We have investigated and characterized the transition to chaos of an axisymmetric 3D bluff-body wake using global LSA and DNS. We have shown that linear stability analysis is an accurate tool to characterize the early transition and the symmetry-breaking sequences. For the axisymmetric wake, the two initial symmetry-breaking bifurcations are associated with spatial symmetry breaking of the rotational symmetry, giving rise to a steady reflectionally symmetric wake, and temporal symmetry breaking, giving rise to unsteady vortex shedding. A fully 3D stability analysis was employed in order to capture accurately the transition from the steady reflectionally symmetric regime to single-frequency vortex shedding.

For higher Reynolds numbers above the unsteady shedding threshold, $\mathrm{Re} > 675$, DNS revealed that the wake preserves the reflectional symmetry. However, intermittent bursts, which interrupt the laminar shedding, were identified. For $\mathrm{Re} > 900$ chaotic behavior is established. The wake breaks the reflectional symmetry and random reorientations in the azimuthal direction occur. Interestingly, the laminar symmetry-breaking instabilities persist even at high Reynolds numbers (Rigas *et al.* 2014, 2015). Future directions of this study involve the use of Lyapunov analysis (Blonigan *et al.* 2016) to extend eigenvalue stability analysis and sensitivity to turbulent regimes.

Acknowledgments

The authors acknowledge use of computational resources from the Certainty cluster awarded by the National Science Foundation to CTR.

REFERENCES

Amestoy, P. R., Duff, I. S., Koster, J. & L'Excellent, J.-Y. 2001 A fully asynchronous multifrontal solver using distributed dynamic scheduling. *SIAM J. Matrix Anal. A.* **23**, 15–41.

Blonigan, P., Fernandez, P., Murman, S., Wang, Q., Rigas, G. & Magri, L. 2016 Towards a chaotic adjoint for LES. *Proceedings of the Summer Program*, Center for Turbulence Research, Stanford University, ??.

Bohorquez, P., Sanmiguel-Rojas, E., Sevilla, A., Jiménez-González, J. I. & Martínez-Bazán, C. 2011 Stability and dynamics of the laminar wake past a slender blunt-based axisymmetric body. *J. Fluid Mech.* **676**, 110–144.

Bottaro, A., Corbett, P. & Luchini, P. 2003 The effect of base flow variation on flow stability. *J. Fluid Mech.* **476**, 293–302.

Brackston, R. D., Garcia de la Cruz, J. M., Wynn, A., Rigas, G. & Morrison, J. F. 2016 Stochastic modelling and feedback control of bistability in a turbulent bluff body wake. *J. Fluid Mech.* **802**, 726–749.

Bury, Y. & Jardin, T. 2012 Transitions to chaos in the wake of an axisymmetric bluff body. *Phys. Lett. A* **376**, 3219–3222.

Fabre, D., Auguste, F. & Magnaudet, J. 2008 Bifurcations and symmetry breaking in the wake of axisymmetric bodies. *Phys. Fluids.* **20**, 051702.

Giannetti, F. & Luchini, P. 2007 Structural sensitivity of the first instability of the cylinder wake. *J. Fluid Mech.* **581**, 167–197.

Grandemange, M., Gohlke, M. & Cadot, O. 2013 Turbulent wake past a three-dimensional blunt body. Part 1. Global modes and bi-stability. *J. Fluid Mech.* **722**, 51–84.

Ham, F., Mattsson, K., Iaccarino, G. & Moin, P. 2007 Towards time-stable and accurate LES on unstructured grids. In *Complex Effects in Large Eddy Simulations*, pp. 235–249. Springer.

Hecht, F. 2012 New development in FreeFem++. *J. Numer. Math.* **20**, 251–266.

Hegger, R., Kantz, H. & Schreiber, T. 1999 Practical implementation of nonlinear time series methods: The TISEAN package. *Chaos* **9**, 413–435.

Hernandez, V., Roman, J. E. & Vidal, V. 2005 SLEPc: A scalable and flexible toolkit for the solution of eigenvalue problems. *ACM T. Math. Software.* **31**, 351–362.

Lin, N., Reed, H. L. & Saric, W. S. 1992 Effect of leading-edge geometry on boundary-layer receptivity to freestream sound. *ICASE NASA.* pp. 421–440.

Luchini, P. & Bottaro, A. 2014 Adjoint equations in stability analysis. *Annu. Rev. Fluid Mech.* **46**, 1–30.

Magri, L. 2015 *Adjoint methods in thermo-acoustic and combustion instability.* PhD thesis, University of Cambridge.

Magri, L., Bauerheim, M. & Juniper, M. P. 2016 Stability analysis of thermo-acoustic nonlinear eigenproblems in annular combustors. Part I. Sensitivity. *J. Comp. Phys.* **325**, 395–410.

Mantič-Lugo, V., Arratia, C. & Gallaire, F. 2014 Self-consistent mean flow description of the nonlinear saturation of the vortex shedding in the cylinder wake. *Phys. Rev. Lett.* **113**, 084501.

Marquet, O. & Larsson, M. 2015 Global wake instabilities of low aspect-ratio flat-plates. *Eur. J. Mech. B-Fluid.* **49**, 400 – 412.

Marquet, O., Sipp, D. & Jacquin, L. 2008 Sensitivity analysis and passive control of cylinder flow. *J. Fluid Mech.* **615**, 221–252.

Meliga, P., Chomaz, J. & Sipp, D. 2009 Global mode interaction and pattern selection in the wake of a disk: a weakly nonlinear expansion. *J. Fluid Mech.* **633**, 159–189.

Oxlade, A. R., Morrison, J. F., Qubain, A. & Rigas, G. 2015 High-frequency forcing of a turbulent axisymmetric wake. *J. Fluid Mech.* **770**, 305–318.

Rigas, G., Morgans, A. S., Brackston, R. D. & Morrison, J. F. 2015 Diffusive dynamics and stochastic models of turbulent axisymmetric wakes. *J. Fluid Mech.* **778**, R2.

Rigas, G., Oxlade, A. R., Morgans, A. S. & Morrison, J. F. 2014 Low-dimensional dynamics of a turbulent axisymmetric wake. *J. Fluid Mech.* **755**, R5.

Sanmiguel-Rojas, E., Jiménez-González, J. I., Bohorquez, P., Pawlak, G. & Martínez-Bazán, C. 2011 Effect of base cavities on the stability of the wake behind slender blunt-based axisymmetric bodies. *Phys. Fluids.* **23**, 114103.

Sipp, D. & Lebedev, A. 2007 Global stability of base and mean flows: a general approach and its applications to cylinder and open cavity flows. *J. Fluid Mech.* **593**, 333–358.

Sipp, D., Marquet, O., Meliga, P. & Barbagallo, A. 2010 Dynamics and control of global instabilities in open-flows: a linearized approach. *Appl. Mech. Rev.* **63**, 030801.

Sipp, D. & Schmid, P. J. 2016 Linear closed-loop control of fluid instabilities and noise-induced perturbations: A review of approaches and tools. *Appl. Mech. Rev.* **68**, 020801.